Water Practice & Technology

IWA PUBLISHING

Water Practice & Technology Vol 18 No 6, 1465 doi: 10.2166/WPT.2023.096

Study of malachite green dye biosorption on acerola (*Malpighia emarginata*) seeds for the treatment of coloured wastewater: kinetics, equilibrium, and experimental design

Antonio José Ferreira Gadelha *, Clarice Oliveira da Rocha, Marcelo Rodrigues do Nascimento, Luellen Pereira Rocha, David Aragão de Sousa and Bernardo Vale da Cunha

Instituto Federal de Educação, Ciência e Tecnologia da Paraíba - IFPB - Campus Campina Grande, Av. Tranquilino Lemos, 671, Campina Grande, Paraíba 58432300, Brazil
*Corresponding author. E-mail: antonio.gadelha@ifpb.edu.br

AJFG, 0000-0002-1930-427X; CO daR, 0000-0002-6335-9163

ABSTRACT

In this work, malachite green dye was removed from an aqueous effluent using acerola seed as an adsorbent. The adsorbent was characterized by Fourier transform infrared (FTIR), X-ray diffraction, zero charge potential, and acid group concentration techniques. The findings revealed that the adsorbent has a characteristic composition of lignocellulosic materials, as described by the FTIR data, besides having a pH-PZC of 3.5 and a concentration of acid groups of 0.2313 mmol g^{-1}. The central composite design was used for batch experiments, and the effects of three variables were analysed. The optimum conditions (pH, particle size, and adsorbent mass) were 10.0, 600 μm, and 0.8 g, respectively, for 97.52% dye removal. Redlich–Peterson isotherm fitted well to the experimental data ($R^2 = 0.997$ and root-mean-square error (RMSE) = 1.168). From the Langmuir isotherm, the maximum adsorption capacity obtained for dye was 103.50 mg g^{-1}. As for the adsorption kinetics, it was found that the pseudo-second-order model sufficiently describes the experimental data ($R^2 = 0.999$ and RMSE = 0.018). Thus, the acerola seed has excellent properties as an adsorbent, demonstrating a remarkable performance and a great capacity to be used in the treatment of aqueous effluents contaminated by dyes.

Key words: adsorption, dye removal, equilibrium isotherms, factorial design, kinetic models, lignocellulosic waste

HIGHLIGHTS

- Biosorption has been investigated as a solution for malachite green dye from wastewater.
- Optimization of dye removal on acerola seed was studied through three factors central composite design.
- The highest removal yield was for adsorbent mass 0.8 g, pH 10.0, and particle size 600 μm.
- From the Langmuir isotherm, the maximum adsorption capacity was 103.5 mg/g. The kinetic data were well fitted by the pseudo-second-order model.

GRAPHICAL ABSTRACT

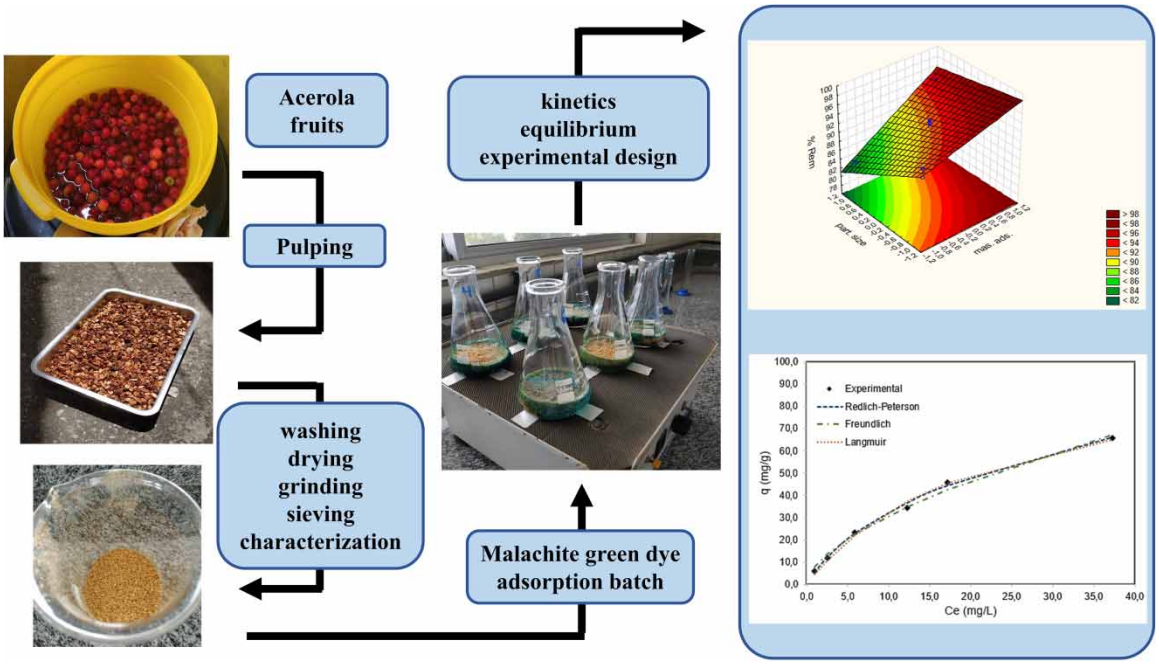

INTRODUCTION

Water is used in almost all human functional operations. It is a crucial factor for both domestic and industrial activities. However, it is common to find water bodies contaminated with plastic waste, toxic products, and other materials that pose a risk to the aquatic balance.

One of the main causes of water pollution is effluents from industrial activities, including toxic chemicals and pollutants, which are improperly disposed of in the environment, in water bodies such as rivers, lakes, aquifers, wells, and oceans.

Dyes are among the most common hazardous environmental pollutants in contaminated water, and they are improperly disposed of due to various industrial activities such as textiles, tanning, pulp and paper, paints, and pigments (Sridhar *et al.* 2022).

Currently, more than 10,000 commercial dyes are available, with an estimated production of 10^6 tons per year (Bulgariu *et al.* 2019). However, a significant amount (>15%) is lost due to the dyeing process, which is discharged as effluent, posing a major threat to living beings and the environment (Dutta *et al.* 2014). This loss corresponds to approximately 280 kilotons of dyes lost in wastewater annually (Mishra *et al.* 2021).

The presence of dyes in water bodies causes distinct changes in water colour with a sudden reduction in oxygen content, harming flora and fauna (Bulgariu *et al.* 2019), impeding light penetration, and slowing photosynthetic activity. Due to their stable chemical structure containing aromatic rings, it is challenging to degrade such complex compounds (Hynes *et al.* 2020). Thus, there is a pressing need for the effective removal of these hazardous compounds to address environmental safety and toxicity.

Dye remediation techniques can be classified into four categories: physical, chemical, physicochemical, and biological. Numerous technologies have been proposed for the treatment of effluents contaminated with dyes: membrane filtration (the physical method) (Song *et al.* 2019); oxidation/Fenton process (the chemical method) (Patel *et al.* 2020); ozonation (Suryawan *et al.* 2018); photocatalytic methods (Kuvarega *et al.* 2018); coagulation/flocculation (Rodrigues *et al.* 2013) and adsorption (Madan *et al.* 2019) (physicochemical methods); and enzymes/microorganisms (Liu *et al.* 2020) and biosorption/biodegradation (Geed *et al.* 2019) (biological techniques). However, most of these dye removal techniques have challenges and drawbacks in terms of cost, generation of hazardous by-products, high energy consumption, efficiency, sustainability, and use of toxic chemicals.

Notably, adsorption procedures are an alternative to treat wastewater containing dyes, which, in turn, have gained prominence among the physicochemical procedures, as it is the one that allows the recovery of the material used, has high efficiency, and is relatively lower cost compared to other technologies.

The application of natural, ecological, and low-cost adsorbents to remove dyes and pigments from aqueous effluents through adsorption has been presented as a promising alternative for the problems generated by these wastes. The use of agro-industrial residues to remove these contaminants has been investigated, considering that these by-products of the agri-food sector represent an abundant, effective, and low-cost source to solve the problem of colour removal in contaminated effluents.

Thus, the production of alternative adsorbent materials has been explored, and among the raw materials used, fruit peels, flowers, seeds, or vegetable parts can be highlighted, mainly because they are reused waste from agricultural activities without any added economic value, which includes *Moringa oleifera* seed (Çelekli *et al.* 2019), mango leaf powder (Uddin & Rahman 2017), pineapple peel (Chaiyaraksa *et al.* 2019), and coffee husk (Murthy *et al.* 2019).

Acerola (*Malpighia emarginata*) is a fruit native to tropical Americas, also called Antilles cherry, and of great economic interest due to its high content of vitamin C. Brazil is the leading country in its production, consumption, and exportation. Acerola fruits are primarily used in the food industry to produce juice, ice cream, liqueur, soft drinks, gum, fruit conserve, jelly, yogurt, and others. With the increase in production, a great amount of fruit waste is generated, reaching up to 40% of the total volume processed, commonly consisting of peel, seed, and bagasse waste rejected during the process. The disposal of these residues is costly for companies, often being discharged or underused, thereby representing significant losses of feedstock and energy resources (Silva *et al.* 2018, 2020).

This article aims to study the use of acerola (*M. emarginata*) seeds in the removal of malachite green dye from aqueous effluents through adsorption in a finite batch, investigating kinetic and equilibrium aspects and the influence of process variables.

METHODS

Materials

Acerola seeds were obtained from the pulping of fruits collected from plants in Lagoa Seca, Paraíba State, Brazil. Analytical grade Malachite Green Oxalate, C.I. 42000 (molecular formula: $C_{46}H_{50}N_4{\cdot}2\ C_2HO_4{\cdot}C_2H_2O_4$; molecular weight: 927.03 g/mol and λ_{max}: 617 nm), sodium hydroxide, hydrochloric acid, and sodium chloride (Neon, Brazil) solutions were prepared in deionized water. The standard dye solution used in the experiments was prepared after stepwise dilution of 1,000 mg L^{-1} stock solution. To determine the dye concentration, a straight-line calibration curve was used, previously prepared by plotting absorbance versus malachite green concentration. The absorbance was measured with a VIS spectrophotometer (WebLaborSP, WUV-M51) at 617 nm wavelength.

Preparation of adsorbent

Acerola seeds were manually cleaned to remove foreign materials and dried in the sunlight for 8 h to remove moisture. Dried acerola seeds were ground in a knife mill and sieved to obtain uniform-sized particles. Grounded acerola seeds were washed repeatedly with distilled water until neutral pH and dried at 60 °C for 12 h.

Point of zero charge and acid group concentrations

The experiments to determine the point of zero charge (PZC) were carried out with 0.1 M NaCl solutions in Erlenmeyer flasks, whose pH values were previously adjusted to 2 and 12, with intervals of 2 units by adding 0.1 M HCl or NaOH solutions. In each flask, 0.1 g of adsorbent was added under stirring at 120 rpm. After 24 h of contact, the samples were decanted, and the pH was measured in the final liquid phases with a Simpla PH-140 pH meter. The PZC was determined by plotting ($pH_{initial} - pH_{final}$) against $pH_{initial}$.

To determine the acid group concentrations, 0.5 g of adsorbent was put in contact with 25 mL of 0.025 M NaOH solution and stirred for 24 h at 100 rpm and 25 °C. Then, the samples were decanted, and the excess base in the final liquid phases was titrated with 0.025 M HCl to determine the surface acidity. The tests were performed in duplicate.

X-ray diffractions

X-ray diffraction (XRD) powder diffraction pattern was obtained from a Bruker – D2 Phaser X-ray diffractometer operated with a voltage of 30 kV, X-ray source Cu kα radiation ($\lambda = 1.5418$ Å), and emission current of 10 mA. The diffractogram was recorded in terms of 2θ in the range of 3.0–70.0° with a step size of 0.02°.

Infrared spectroscopy

The infrared (IR) spectra in the 4,000–500 cm^{-1} range were obtained for the adsorbent at room temperature using a Bruker VERTEX-70 Fourier transform infrared (FTIR), with a resolution of 4 cm^{-1}. The samples were prepared using the standard KBr pellet method.

Adsorption isotherms

Batch adsorption studies were carried out in 125 mL Erlenmeyer flasks. Firstly, 0.1 g of the adsorbent was put in contact with 50 mL of malachite green solutions (pH 5.5) of different concentrations (25, 50, 100, 150, 200, 300, 400, and 500 mg L^{-1}). The contents were agitated on an orbital shaker at 100 rpm for 30 min at room temperature. Afterwards, 10-mL samples of the solution were filtered through filter paper, and the residual dye concentration was measured by visible spectrophotometry at 617 nm. The dye removal efficiency was given by the percentage of dye removal and adsorption capacity, calculated using Equations (1)–(3):

$$\%\text{Rem} = \frac{(C_0 - C_t)}{C_t} \times 100 \tag{1}$$

$$q_t = \frac{(C_0 - C_t)}{m} \times V \tag{2}$$

$$q_e = \frac{(C_0 - C_e)}{m} \times V \tag{3}$$

where %Rem is the percentage of dye removal, and C_0, C_t, and C_e are the initial concentration, at time t, and final concentration (mg L^{-1}) of malachite green dye in the solution, respectively. q_t and q_e are the adsorption capacities (mg g^{-1}) at time t or equilibrium time, respectively. V is the volume (L) of the solution, and m is the mass (g) of the adsorbent used.

To evaluate the fit of the experimental data, the Langmuir, Freundlich, and Redlich–Peterson isotherms were used, as described by Nascimento *et al.* (2014), using nonlinear regression, from Equations (4)–(6), respectively:

$$q_e = \frac{q_m\, k_L\, C_e}{1 + (k_L\, C_e)} \tag{4}$$

$$q_e = k_F\, C_e^{\frac{1}{nF}} \tag{5}$$

$$q_e = \frac{K_{RP} C_e}{1 + a_{RP} C_e^{\beta}} \tag{6}$$

where q_m is the maximum adsorptive capacity (mg g^{-1}), k_L is the Langmuir constant (L mg^{-1}), k_F is the Freundlich constant ((mg g^{-1}) (mg L^{-1})$^{-1/nF}$), $1/nF$ is the heterogeneity factor (dimensionless), k_{RP} (L mg^{-1}) and a_{RP} (L mg^{-1})$^{\beta}$ are the constants for the Redlich–Peterson model, and β is the exponent of the Redlich–Peterson model (dimensionless).

Adsorption kinetics

Kinetic removal of malachite green dye by acerola seed adsorbent was performed by batch experiments. Samples of 1.5 g of adsorbent, with 850 μm average particle size, and 100 mL aliquot of a 100 mg L^{-1} solution (pH 5.5) were placed in an Erlenmeyer flask and agitated on an orbital shaker at 120 rpm and room temperature (298.15 K). At different time periods (0, 60, 120, 180, 240, 300, 360, 420, 480, 540, and 600 s), aliquots of the supernatant solution were taken, and the malachite green concentration was determined using a visible spectrophotometer ($\lambda = 617$ nm).

The experimental data were evaluated by fitting with pseudo-first-order, pseudo-second-order, second-order (Elovich), and Weber–Morris intraparticle diffusion models, as described by Nascimento *et al.* (2014), through

nonlinear regression, represented by Equations (7)–(10), respectively:

$$q_1 = q_e(1 - \exp(-k_1 t)) \tag{7}$$

$$q_2 = \frac{t}{(1/k_2 q_e^2) + (t/q_e)} \tag{8}$$

$$q_3 = \frac{1}{\beta}\ln(\alpha\beta) + \frac{1}{\beta}\ln(t) \tag{9}$$

$$q_4 = k_{id}\sqrt{t} + C \tag{10}$$

where q_e is the adsorption capacity at equilibrium (mg g^{-1}) and k_1 (min^{-1}), and k_2 (g mg^{-1} min^{-1}) are the constants of the pseudo-first-order and pseudo-second-order models, respectively. q_1, q_2, q_3, and q_4 are the theoretical values of adsorption capacity (mg g^{-1}) at any time, t. α is the initial adsorption rate (mg g^{-1} min^{-1}), and β is the desorption rate (mg g^{-1}). k_{id} is the IPD rate constant (mg/(g.$min^{0.5}$)), and C is the initial adsorption (mg g^{-1}).

Regression analysis of the experimental data was performed using Microsoft Excel (2016) by the nonlinear least square method using the SOLVER tool based on the generalized reduced gradient method. The accuracy of the data fit was measured by evaluating the statistical parameters coefficient of determination (R^2), residual sum of squares (RSS), and root-mean-square error (RMSE).

Experimental design

The adsorption process parameters, i.e., adsorbent mass (X_1), pH (X_2), and average particle size (X_3) were evaluated using a full factorial design, a central composite design (CCD). A total of 11 trials were conducted, comprising 8 factorial runs and 3 central runs (Table 1).

Table 1 | Experimental design of the 11 trials using CCD

Run	Adsorbent mass (g), X_1	pH (dimensionless), X_2	Average particle size (μm), X_3
1	0.2 (−1)	4.0 (−1)	600 (−1)
2	0.8 (+1)	4.0 (−1)	600 (−1)
3	0.2 (−1)	10.0 (+1)	600 (−1)
4	0.8 (+1)	10.0 (+1)	600 (−1)
5	0.2 (−1)	4.0 (−1)	850 (+1)
6	0.8 (+1)	4.0 (−1)	850 (+1)
7	0.2 (−1)	10.0 (+1)	850 (+1)
8	0.8 (+1)	10.0 (+1)	850 (+1)
9	0.5 (0)	7.0 (0)	725 (0)
10	0.5 (0)	7.0 (0)	725 (0)
11	0.5 (0)	7.0 (0)	725 (0)

Source: Elaborated by the authors.

A 50 mL aliquot of malachite green solution (200 mg L^{-1}) was mixed with an adsorbent dosage (Table 1) in a 125 mL Erlenmeyer flask and shaken for 30 min at 120 rpm using an orbital shaker at room temperature. Then, the solutions were filtered through Whatman filter paper No. 41. To determine the malachite green concentration in the final solution, the absorbance of each sample was measured with a VIS spectrophotometer at 617 nm. The response variable was evaluated as the percentage of dye removal (%Rem), shown in Equation (1).

From the results of the CCD runs, a regression model was obtained (Equation (11)), which was evaluated by analysis of variance (ANOVA), p-values, F-values, and coefficient of determination (R^2). The Statistica software (version 10.0) was used to generate the regression model, the response surface, and the Pareto chart.

$$Y = \beta_0 + \beta_1 X_1 + \beta_2 X_2 + \beta_3 X_3 + \beta_{12} X_1 X_2 + \beta_{23} X_2 X_3 + \beta_{13} X_1 X_3 + \beta_{123} X_1 X_2 X_3 \tag{11}$$

where Y is the response variable (percentage of dye removal); X_1, X_2, and X_3 are the independent variables, i.e., the process parameters (adsorbent mass, pH, and particle size); β_0 is the average response in all runs; β_1, β_2, and β_3 are the linear coefficients of the model; β_{12}, β_{13}, and β_{23} are the second-order interaction coefficients; and β_{123} is the third-order interaction coefficient.

RESULTS AND DISCUSSION

Point of zero charge and acid groups concentration

The adsorbent surface charge was evaluated by the determining the pH at the PZC, pH(PZC). From the plot of (initial pH – final pH) versus initial pH, the pH(PZC) was determined by the intersection between the curve and the initial pH axis. Figure 1 illustrates that the pH(PZC) of the acerola grounded seed was 3.5. According to Murthy *et al.* (2019), when pH < pH(PZC), the solid surface is predominantly positive charge and repels dye particles (cationic). In turn, when pH > pH(PZC), the surface has a negative charge, which increases the adsorption rate due to the strong electrostatic force between the adsorbent and the dye molecules, thus favouring the dye adsorption process.

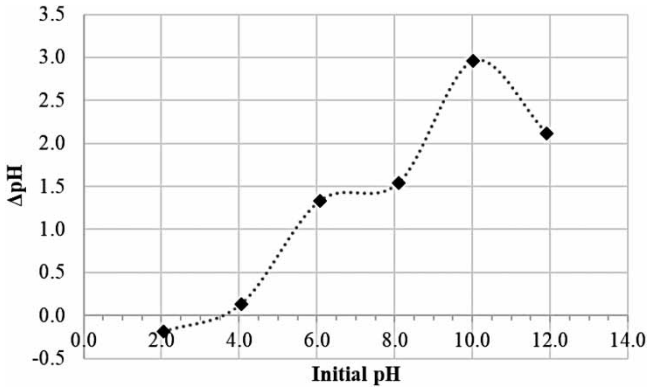

Figure 1 | pH at the point of zero charge of the acerola grounded seed. *Source*: Elaborated by the authors.

Referring to acid group concentration (AGC) on the acerola seed surface, an amount of 0.2313 mmol g^{-1} of adsorbent was obtained. The principal surface acid groups in lignocellulosic materials are the phenolic (-OH), lactone (-C = O), and carboxylic (-COOH) functional groups, responsible for the adsorption of dye molecules, metal ions, etc. Similar results are presented by Nogueira *et al.* (2019), who report that these groups promote interactions between the adsorbate and the adsorbent, making surface complexes, π-bonds, and supporting adsorption.

X-ray diffractions

The X-ray diffractogram of the material formed from the milling of the acerola seed, illustrated in Figure 2, shows a typically organic composition, consequently, amorphous and monophasic materials with some crystallinity, in a discrete way, probably some phase or phases (since it has a multi-peak format) of alkali and/or alkaline earth metals, such as potassium, calcium, magnesium, and sodium, with a non-stoichiometric formula or even some micromineral (micronutrient) of transition.

IR spectroscopy

The IR vibrational spectroscopy technique (Figure 3) was used to identify the structural units of this complex structure based on the vibrational frequencies of the molecules and the short-range organization in the case of inorganic solids, and to verify the presence of chemical species. The interpretation of the spectra provides information on the presence of water or another solvent in the structure of the compounds through the characteristic bands of the species.

According to Silverstein & Webster (1998), the bands in the region of 1,570–1,645 cm^{-1} are characteristic of the carboxylate ion (COO^-); the first intense band comes from the asymmetric axial strain, while the other is weaker and comes from the symmetric axial strain. In this work, these bands are observed at 1,531 and 1,629 cm^{-1}.

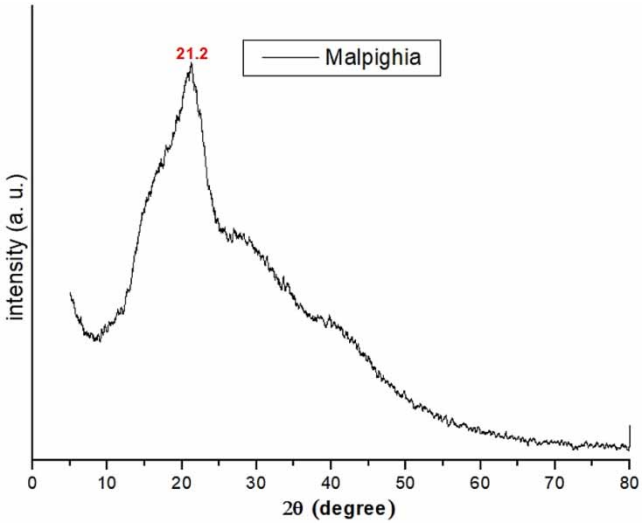

Figure 2 | X-ray diffraction of the ground acerola seed powder. *Source*: Elaborated by the authors.

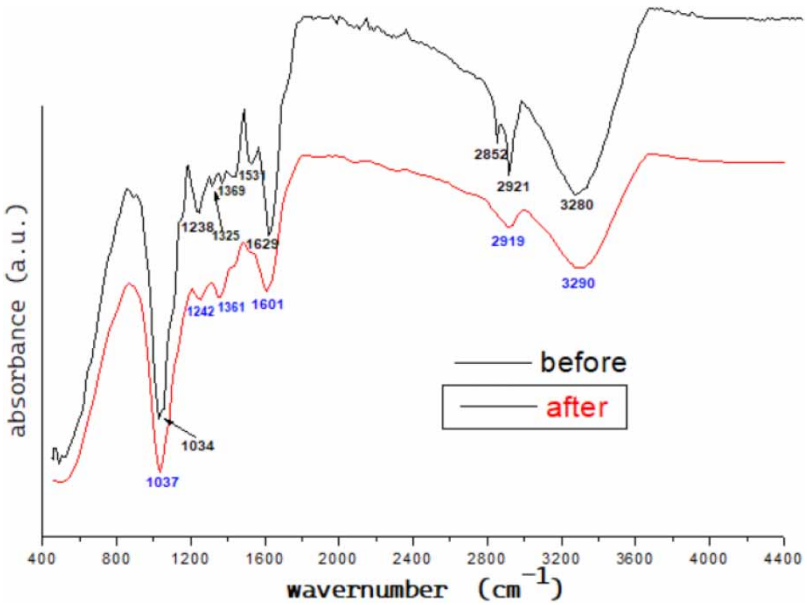

Figure 3 | Infrared spectrum (FTIR) of the ground acerola seed powder. *Source*: Elaborated by the authors.

Nakamoto (1997) found that the hydroxyl group (OH^-) exhibits a metal-OH bonding mode that appears at approximately 1,100 cm^{-1}. In this study, this band appears at 1,034 cm^{-1}, and this displacement occurs due to interactions with other groups and/or bonds.

The broad and intense band 3,280 cm^{-1} can be attributed to the O-H stretching vibration. The two bands located at 2,921 and 2,852 cm^{-1} can be attributed to asymmetric and symmetric -CH_2 stretching vibration, respectively. IR absorption bands at 1,238, 1,325, and 1,369 cm^{-1} can be attributed to the N-H stretching vibration emitted by some aromatic compounds found in the material composition (Silva *et al.* 2020).

The biomass associated with alkali and alkaline earth metals is usually found in bands with high energy, as in this region stretching and bending vibrations can be assigned on the surface of hydroxyl groups. It is not clear from Figure 3 whether a band or shoulder is formed at 488 cm^{-1}.

Analysing the adsorbent spectra, before and after the dye adsorption, it is possible to notice that the broad and intense band 3,280 cm^{-1} suffered a small increment due to the contact with the solution. After adsorption, the peak at 2,852 cm^{-1} merges into a broadband formation at 2,919 cm^{-1}, which is also attributed to the asymmetric and symmetric stretching vibration –CH_2.

The peak 1,531 cm^{-1}, characteristic of the carboxylate ion (COO^{-}), originating from the asymmetric axial strain, disappears after adsorption, while the symmetric axial strain band widens and shifts to 1,601 cm^{-1}. Other smaller bands, due to the N-H stretching vibration (1,238, 1,325, and 1,369 cm^{-1}), also undergo smoothing, forming wider shoulders. These cited modifications do not constitute a visible change in the spectrum profile, making it clear that the structure of the material, at medium range, remains stable.

Adsorption isotherms

Knowing the adsorption, equilibrium provides a basis for evaluating the adsorption process, characterizing the adsorbent/adsorbent interaction, selecting adsorption conditions, and designing the batch.

The adsorption isotherm data were analysed using the Langmuir, Freundlich, and Redlich–Peterson models, described by Equations (4)–(6), respectively. Nonlinear regression analysis, using the nonlinear least square method, was performed to estimate the model parameters, depicted in Table 2.

Table 2 | Statistical parameters of the adsorption isotherm models for malachite green adsorption in acerola seed

					Statistical parameters		
Model	**Temperature (K)**	**Model constants**			R^2	**RSS**	**RMSE**
Langmuir		k_L	q_L				
	298.15	0.046	103.507		0.995	14.580	1.559
Freundlich		k_F	n				
	298.15	7.957	1.696		0.992	20.742	1.859
Redlich–Peterson		k_{RP}	a_{RP}	β			
	298.15	6.036	0.189	0.588	0.997	8.179	1.168

Source: Elaborated by the authors.

Table 2 shows that the R^2 values of the Redlich–Peterson model are closer to unity than the R^2 values of the Langmuir and Freundlich models. Nevertheless, the R^2 values of the three models are greater than 0.99, thus confirming that these models can be applied to explain the malachite green adsorption onto acerola seed. The lower RSS and RMSE values of the Redlich–Peterson model compared to that of the Langmuir and Freundlich models also evidence that the first one better describes the experimental data.

According to Nascimento *et al.* (2014), the empirical Redlich–Peterson equation combines characteristics of the Langmuir and Freundlich models, approaching the former at low concentrations, when β tends to 1, and assuming the form of the latter in systems under high concentrations, when β tends to zero. In this case, as the β value is closer to 1 ($\beta = 0.588$), the Redlich–Peterson statistical parameters are closer to those of the Langmuir model.

In addition, Freundlich isotherms with $1/n > 1$ show relatively high adsorbent loadings at low concentrations. Therefore, they are referred to as favourable isotherms, whereas isotherms with $1/n < 1$ are characterized as unfavourable. This result also indicates that the adsorption process occurs in multilayers.

Figure 4 illustrates the comparison between the experimental data and the model-calculated values of adsorption capacity for the Langmuir, Freundlich, and Redlich–Peterson models. The Langmuir model revealed a maximum adsorption capacity of 103.507 mg g^{-1}. In comparison, Murthy *et al.* (2019) reported values of adsorptive capacity for different adsorbents: H_2SO_4-treated coffee husk (264.812 mg g^{-1}), NaOH-modified grapefruit peel (314.90 mg g^{-1}), EDTA-modified sugarcane bagasse (157.2 mg g^{-1}). Furthermore, Mishra *et al.* (2021) showed adsorptive capacities for other materials: *M. oleifera* seed husk (91.74 mg g^{-1}) and *Theobroma grandiflorum* seed shell (64.1 mg g^{-1}).

Adsorption kinetics

According to Murthy *et al.* (2019), the kinetics of the adsorption process allows to describe the rate of uptake of adsorbent, which, in turn, determines the contact time of the adsorption required for reaching equilibrium.

The experimental data obtained were fitted to four different kinetic models, i.e., pseudo-first-order, pseudo-second-order, second-order (Elovich), and Weber–Morris IPD models, described by Equations (7)–(10), respectively.

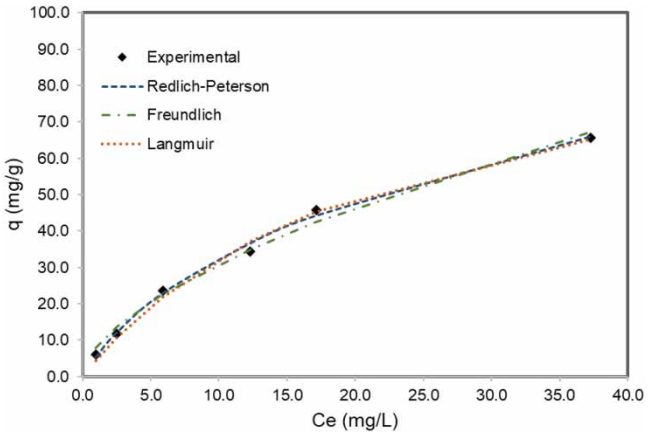

Figure 4 | Adsorption isotherms for malachite green dye onto acerola seed. *Source*: Elaborated by the authors.

Kinetic and statistical parameters obtained by nonlinear regression using the least squares method are summarised in Table 3.

Table 3 | Adsorption kinetics model and statistical parameters for malachite green adsorption in acerola seed

				Statistical parameters		
Model	**Concentration (g L^{-1})**	**Model constants**		R^2	**RSS**	**RMSE**
Pseudo-first order		q_1	k_1			
	100.0	6.240	0.036	0.998	0.064	0.077
Pseudo-second order		q_2	k_2			
	100.0	6.426	0.017	0.999	0.004	0.018
Second order		α	β			
	100.0	698.293	3.289	0.996	0.053	0.070
Weber–Morris IPD		k_{id}	C			
	100.0	0.197	2.479	0.607	13.745	1.118

Source: Elaborated by the authors.

The R^2 values for all three models are very close to unity, which shows that they all explain the experimental data satisfactorily well. However, the pseudo-second-order model still presents a higher value than the other models, which implies that it fits better with the experimental kinetic data. The lower RSS and RMSE values of the pseudo-second-order model compared to that of the pseudo-first-order and Elovich models also demonstrate that the first one better describes the experimental data.

The pseudo-second-order model assumes that there is more than one controlling step in the adsorption process, such as external and internal diffusion, in addition to diffusion at the active site itself. In this case, the rate constant k_2 is equal to 0.017 g/mg s. It also considers that adsorption occurs at localized sites and does not involve interaction between adsorbate particles. Moreover, the maximum adsorption corresponds to a saturated monolayer of adsorbate on the surface of the adsorbent.

Figure 5 illustrates the comparison between the experimental data and the calculated values of adsorption capacity for the kinetics models.

Pseudo-first-order and pseudo-second-order models are not sufficient to explain the adsorption mechanism. Therefore, the Weber–Morris intraparticle diffusion model was used to identify the rate-controlling step. Figure 6 shows the plot between q and t fitting the experimental and Weber–Moris IPD equation.

Internal diffusion models assume that mass transfer into the interior of the particle is the slowest step in the adsorption process. When the adsorption process is controlled only by the intraparticle diffusion mechanism, the line should pass through the origin. In this work, the intercept of the plot occurs above the origin, which

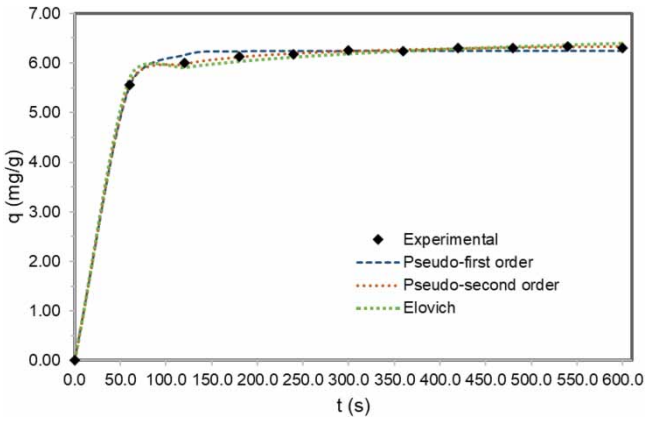

Figure 5 | Adsorption kinetics for malachite green dye onto acerola seed. *Source*: Elaborated by the authors.

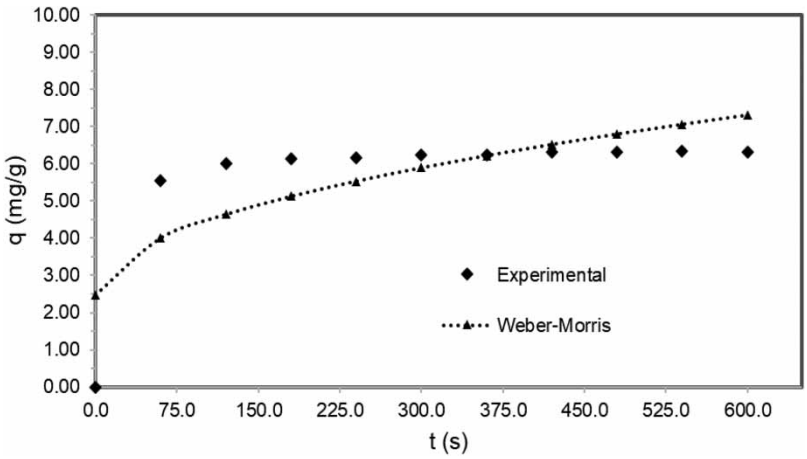

Figure 6 | Experimental and modelled kinetics adsorption by Weber–Morris equation for the malachite green dye onto acerola seed. *Source*: Elaborated by the authors.

implies multi-linearity, thus indicating that the adsorption process is controlled by multiple steps, i.e., the intra-particle diffusion is not the only rate-limiting step.

Experimental design

Independent variables such as adsorbent mass (X_1), pH (X_2), and average particle size (X_3) were statistically evaluated using a CCD to investigate their effects on the response of interest, the percentage of dye removal (%Rem). A first-order polynomial model was fitted to the experimental results of malachite green removal using Statistica 10.0 software. The model obtained is shown in Equation (12):

$$Y = 91.90 + 4.36X_1 + 0.59X_2 - 3.01X_3 - 0.40X_1X_2 + 1.39X_1X_3 + 0.02X_2X_3 \quad (12)$$

The experimental and predicted results (using Equation (10)) for dye removal of each experimental trial are listed in Table 4.

The ANOVA shown in Table 5 was used to assess the significance and adequacy of the model. Statistical analysis of data variance was performed using Fisher's *F*-test.

To evaluate the significance of the regression model, the determination coefficient, R^2, was used. When R^2 assumes values closer to 1, this indicates a better model prediction. In this case, the ANOVA shows that the adequacy between the experimental and the predicted values is high, with an R^2 value of 0.9671 for dye removal onto acerola seed. This result indicates that 96.71% of the total data variance can be explained by the three independent variables analysed, showing the high degree of fit of the model.

Table 4 | CCD results for the experimental and predicted values for malachite green removal

Run	Adsorbent mass (g), X_1	pH (dimensionless), X_2	Average particle size (μm), X_3	Dye removal (%)	
				Predicted	Experimental
1	0.2 (−1)	4.0 (−1)	600 (−1)	90.97	90.44
2	0.8 (+1)	4.0 (−1)	600 (−1)	97.72	97.19
3	0.2 (−1)	10.0 (+1)	600 (−1)	92.90	92.38
4	0.8 (+1)	10.0 (+1)	600 (−1)	98.05	97.52
5	0.2 (−1)	4.0 (−1)	850 (+1)	82.13	81.60
6	0.8 (+1)	4.0 (−1)	850 (+1)	94.42	93.90
7	0.2 (−1)	10.0 (+1)	850 (+1)	84.15	83.63
8	0.8 (+1)	10.0 (+1)	850 (+1)	94.84	94.31
9	0.5 (0)	7.0 (0)	725 (0)	91.90	93.62
10	0.5 (0)	7.0 (0)	725 (0)	91.90	93.09
11	0.5 (0)	7.0 (0)	725 (0)	91.90	93.20

Source: Elaborated by the authors.

Table 5 | Analysis of variance for the CCD design for the malachite green adsorption study

Source	Sum of squares (SS)	Degrees of freedom	Mean square	*F*-value	*p*-value
Adsorbent mass (X_1)	152.07	1	152.07	1,974.43	0.0005*
pH (X_2)	2.76	1	2.76	35.83	0.0268*
Particle size (X_3)	72.58	1	72.58	942.33	0.0011*
$\boldsymbol{X_1X_2}$	1.30	1	1.30	16.86	0.0545
$\boldsymbol{X_1X_3}$	15.36	1	15.36	199.40	0.0049*
$\boldsymbol{X_2X_3}$	0.004	1	0.004	0.05	0.8393
Lack of fit	8.16	2	4.08	52.98	0.0185*
Pure error	0.15	2	0.08		
Total SS	252.39	10			

*p-Value < 0.05 indicates that the model terms are significant.
Source: Elaborated by the authors.

According to Alam *et al.* (2022), the model and its terms can be considered statistically significant when the *p*-value is less than 0.05 with a larger *F*-value. The finds revealed that the linear terms, adsorbent mass (X_1), pH (X_2), and particle size (X_3) showed the most significant effect with p-value < 0.05 and higher values for F. The interactive term between adsorbent mass and particle size (X_1X_3) was also significant ($p < 0.05$), while the other two interactive terms adsorbent mass and pH (X_1X_2) and pH and particle size (X_2X_3) were not significant in the range analysed. This is corroborated by the Pareto chart presented in Figure 7, which shows the standardized effects for each term in the model.

Thus, a slight variation (independent variables) in the operational conditions promotes a significant alteration in the response, malachite green removal. In this case, the lack of fit of the model appears to be significant. However, this is due to the small value found for the pure error, with which the lack of fit is quantified.

To determine the optimal values for dye removal, the regression model equation was illustrated by 3D response surface and 2D contour plots for the studied variables within the experimental ranges.

The effects of adsorbent mass and pH are presented in Figure 8. The 3D response surface and 2D plot contours show that the malachite dye removal is significantly affected by varying adsorbent mass and pH of the solution. Higher values for the response variable can be obtained at higher values for the adsorbent mass and pH. Dye removal increased with increasing adsorbent mass, from 86% at 0.2 g to 96% at 0.8 g. The pH effect agrees with the pH analysis at the PZC, indicating that at higher pH values, the adsorption of cationic dyes is favoured by electrostatic interaction with surface charges.

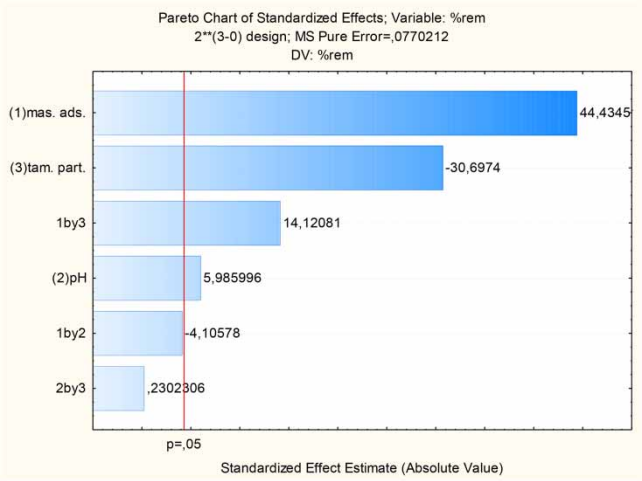

Figure 7 | Pareto chart of standardized effects for malachite green adsorption onto acerola seed. *Source*: Elaborated by the authors.

However, as described by ANOVA and the Pareto chart, the effect of pH on dye removal is less than the influence of adsorbent mass, as shown in Figure 8.

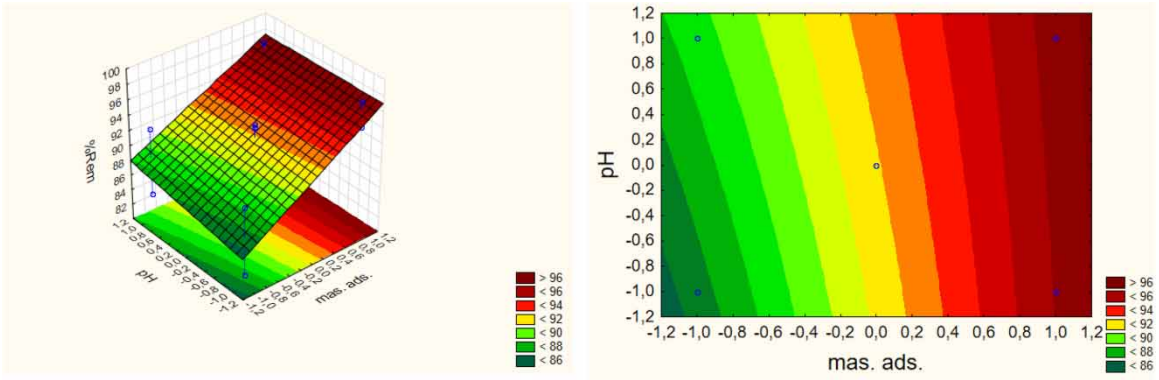

Figure 8 | 3D response surfaces and 2D contour plots show the effect of adsorbent mass and pH on malachite green removal (%Rem). *Source*: Elaborated by the authors.

Figure 9 displays the interaction between pH and average particle size of the adsorbent. The smaller the particle size and the higher the pH, the higher the percentage of dye removal. This finding agrees with the Pareto

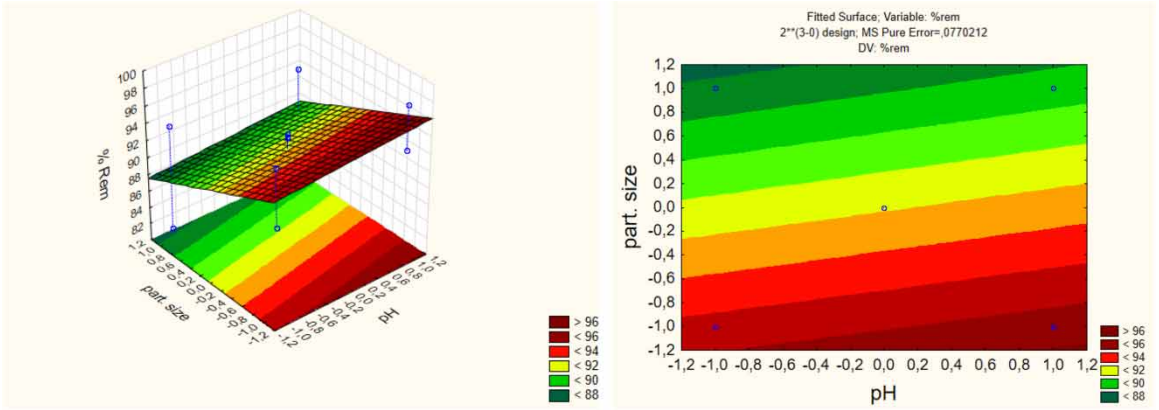

Figure 9 | 3D response surfaces and 2D contour plots show the effect of average particle size and pH on malachite green removal (%Rem). *Source*: Elaborated by the authors.

diagram and the regression model obtained from ANOVA, which has a negative sign for the particle size variable. The particle size has a greater effect than pH on the response variable, ranging from <88% removal at 850 μm to >96% removal at 600 μm.

The interaction effects between the most significant process variables (adsorbent mass and particle size) are shown in Figure 10. In this case, maximum removal is achieved when using higher values of adsorbent mass and lower values of particle size. Dye removal greater than 98% can be achieved when 0.8 g of adsorbent with an average particle size of 600 μm is used.

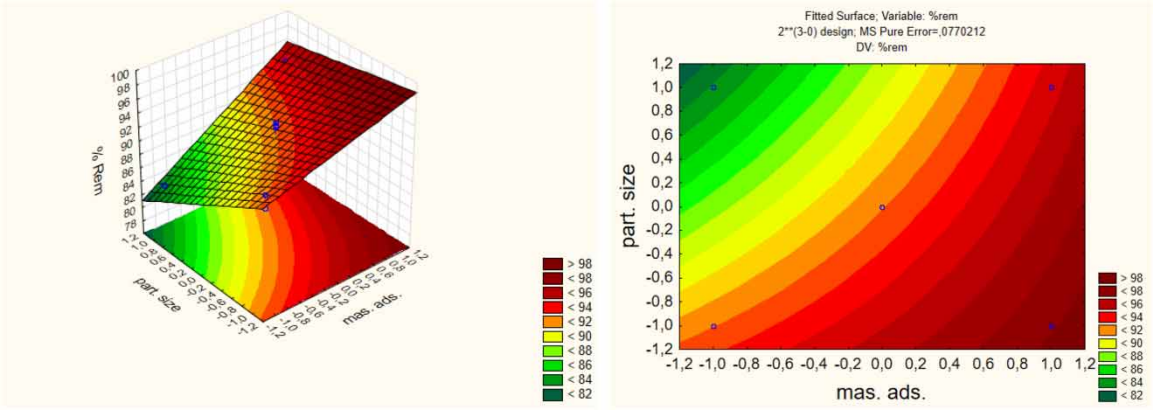

Figure 10 | 3D response surfaces and 2D contour plots show the effect of average particle size and adsorbent mass on malachite green removal (%Rem). *Source*: Elaborated by the authors.

CONCLUSIONS

Locally, acerola seeds were investigated as an adsorbent for the removal of malachite green dye from synthetic wastewater. The adsorbents were characterized by XRD, FTIR spectroscopy, pH-PZC, and AGC techniques. The kinetic adsorption of malachite green onto acerola seeds follows the pseudo-second-order model. The intraparticle diffusion mechanism indicates the adsorption process is controlled by multiple steps, showing that the intraparticle diffusion is not the only rate-limiting step. The Redlich–Peterson isotherm model better fitted the equilibrium data. Adsorbent mass, pH, and average particle size were evaluated as process parameters for dye adsorption onto acerola seed. These independent variables were investigated by a statistical experimental design (CCD), and all three were statistically significant, with particle size and adsorbent mass having the greatest effects on dye removal. The optimal conditions (pH, particle size, and adsorbent mass) were 10.0, 600 μm, and 0.8 g, respectively, for 97.52% dye removal. The results suggest that grounded acerola seed has a good adsorption capacity and is a promising and low-cost adsorbent material for dye removal from industrial effluents. A possible way of concentrating and recovering malachite green dye adsorbed on acerola seed would be through dye solubilization in an organic solvent, such as methanol. This proposal involves drying the adsorbent solid containing the adsorbed dye, mixing it with methanol under stirring for a certain period, filtration to recover the dye-free adsorbent. Finally, the methanol containing the dissolved dye is separated by vacuum evaporation, regenerating the dye.

DATA AVAILABILITY STATEMENT

All relevant data are included in the paper or its Supplementary Information.

CONFLICT OF INTEREST

The authors declare there is no conflict.

REFERENCES

Alam, M., Bari, M. N. & Kawsari, S. 2022 Statistical optimization of methylene blue dye removal from a synthetic textile wastewater using indigenous adsorbents. *Environmental and Sustainability Indicators* **14**, 100176. https://doi.org/10.1016/j.indic.2022.100176.

Bulgariu, L., Escudero, L. B., Bello, O. S., Iqbal, M., Nisar, J., Adegoke, K. A., Alakhras, F., Kornaros, M. & Anastopoulos, I. 2019 The utilization of leaf-based adsorbents for dyes removal: a review. *Journal of Molecular Liquids* **276**, 728–747. https://doi.org/10.1016/j.molliq.2018.12.001.

Çelekli, A., Al-Nuaimi, A. I. & Bozkurt, H. 2019 Adsorption kinetic and isotherms of Reactive Red 120 on *Moringa oleifera* seed as an eco-friendly process. *Journal of Molecular Structure* **1195**, 168–178. https://doi.org/10.1016/j.molstruc.2019.05.106.

Chaiyaraksa, C., Ruenroeng, C., Buaphuan, B. & Choksakul, S. 2019 Adsorption of cationic and anionic dye using modified pineapple peel. *Songklanakarin Journal of Science & Technology* **41**(1), 199–206.

Dutta, R., Nagarjuna, T. V., Mandavgane, S. A. & Ekhe, J. D. 2014 Ultrafast removal of cationic dye using agrowaste-derived mesoporous adsorbent. *Industrial & Engineering Chemistry Research* **53**(48), 18558–18567. https://doi.org/10.1021/ie5030003.

Geed, S. R., Samal, K. & Tagade, A. 2019 Development of adsorption-biodegradation hybrid process for removal of methylene blue from wastewater. *Journal of Environmental Chemical Engineering* **7**(6), 103439. https://doi.org/10.1016/j.jece.2019.103439.

Hynes, N. R. J., Kumar, J. S., Kamyab, H., Sujana, J. A. J., Al-Khashman, O. A., Kuslu, Y., Ene, A. & Suresh Kumar, B. 2020 Modern enabling techniques and adsorbents-based dye removal with sustainability concerns in textile industrial sector – a comprehensive review. *Journal of Cleaner Production* **272**, 122–636. https://doi.org/10.1016/j.jclepro.2020.122636.

Kuvarega, A. T., Khumalo, N., Dlamini, D. & Mamba, B. B. 2018 Polysulfone/N,Pd co-doped TiO_2 composite membranes for photocatalytic dye degradation. *Separation and Purification Technology* **191**, 122–133. https://doi.org/10.1016/j.seppur.2017.07.064.

Liu, S., Xu, X., Kang, Y., Xiao, Y. & Liu, H. 2020 Degradation and detoxification of azo dyes with recombinant ligninolytic enzymes from *Aspergillus* sp. with secretory overexpression in *Pichia pastoris*. *Royal Society Open Science* **7**(9), 200688. https://doi.org/10.1098/rsos.200688.

Madan, S., Shaw, R., Tiwari, S. & Tiwari, S. K. 2019 Adsorption dynamics of Congo Red dye removal using ZnO functionalized high silica zeolitic particles. *Applied Surface Science* **487**, 907–917. https://doi.org/10.1016/j.apsusc.2019.04.273.

Mishra, S., Cheng, L. & Maiti, A. 2021 The utilization of agro-biomass/byproducts for effective bio-removal of dyes from dyeing wastewater: a comprehensive review. *Journal of Environmental Chemical Engineering* **9**(1), 1–22. https://doi.org/10.1016/j.jece.2020.104901.

Murthy, T. P. K., Gowrishankar, B. S., Prabha, M. N. C., Kruthi, M. & Krishna, R. H. 2019 Studies on batch adsorptive removal of malachite green from synthetic wastewater using acid treated coffee husk: equilibrium, kinetics and thermodynamic studies. *Microchemical Journal* **146**, 192–201. https://doi.org/10.1016/j.microc.2018.12.067.

Nakamoto, K. 1997 *Infrared and Raman Spectra of Inorganic and Coordination Compounds*. John Wiley & Sons, New York.

Nascimento, R. F., Lima, A. C. A., Vidal, C. B., Melo, D. D. Q. & Raulino, G. S. C. 2014 *Adsorção: aspectos teóricos e aplicações ambientais*. Imprensa Universitária – UFC, Fortaleza.

Nogueira, G. D. R., Souza, B. A., Silva, P. B., Duarte, C. R. & Barrozo, M. A. S. 2019 Caracterização e aplicação do hidrocarvão obtido a partir da carbonização hidrotérmica do resíduo de acerola (*Malphigia emarginata* D.C.). (2019 Characterization and application of hydrocarbon obtained from hydrothermal carbonization of acerola (*Malphigia emarginata* D.C.) residue). In *XXXIX Congresso Brasileiro de Sistemas Particulados*, October 27–30, Belém.

Patel, S. K., Patel, S. G. & Patel, G. V. 2020 Degradation of reactive dye in aqueous solution by fenton, photo-Fenton process and combination process with activated charcoal and TiO_2. *Proceedings of the National Academy of Sciences, India Section A: Physical Sciences* **90**, 579–591. https://doi.org/10.1007/s40010-019-00618-3.

Rodrigues, C. S. D., Madeira, L. M. & Boaventura, R. A. R. 2013 Treatment of textile dye wastewaters using ferrous sulphate in a chemical coagulation/flocculation process. *Environmental Technology* **34**(6), 719–729. https://doi.org/10.1080/09593330.2012.715679.

Silva, A. C. P., Jorgetto, A. O., Wondracek, M. H. P., Galera, R. M., Schneider, J. F., Saeki, M. J., Pedrosa, V. A., Zara, L. F. & Castro, G. R. 2018 Properties, characteristics and application of grinded *Malpighia emarginata* seeds in the removal of toxic metals from water. *Groundwater for Sustainable Development* **6**, 50–56. http://dx.doi.org/10.1016/j.gsd.2017.10.006.

Silva, J. D. O., Santos, D. E. L., Abud, A. K. S. & Oliveira Júnior, A. M. 2020 Characterization of acerola (*Malpighia emarginata*) industrial waste as raw material for thermochemical processes. *Waste Management* **107**, 143–149. https://doi.org/10.1016/j.wasman.2020.03.037.

Silverstein, R. M. & Webster, F. X. 1998 *Identificação espectrométrica de compostos orgânicos*, 6th edn. LTC editora, Rio de Janeiro.

Song, Y., Seo, J. Y., Kim, H. & Beak, K. Y. 2019 Structural control of cellulose nanofibrous composite membrane with metal organic framework (ZIF-8) for highly selective removal of cationic dye. *Carbohydrate Polymer* **222**, 115018. https://doi.org/10.1016/j.carbpol.2019.115018.

Sridhar, A., Ponnuchamy, M., Kapoor, A. & Prabhakar, S. 2022 Valorization of food waste as adsorbents for toxic dye removal from contaminated waters: a review. *Journal of Hazardous Materials* **424**(127432), 1–27. https://doi.org/10.1016/j.jhazmat.2021.127432.

Suryawan, I. W. K., Helmy, Q. & Notodarmojo, S. 2018 Textile wastewater treatment: colour and COD removal of reactive black-5 by ozonation. In: *IOP Conference Series: Earth and Environmental Science*. Institute of Physics Publishing. Vol. 106, August 9–10, 2017, Jakarta, p. 12102. https://doi.org/10.1088/1755-1315/106/1/012102.

Uddin, M. T. & Rahman, M. A. 2017 A potential low-cost adsorbent for the removal of cationic dyes from aqueous solutions. *Applied Water Science* **7**, 2831–2842. https://doi.org/10.1007/s13201-017-0542-4.

First received 12 February 2023; accepted in revised form 4 June 2023. Available online 16 June 2023